TRANSPLANTATION

Resident memory T cells form during persistent antigen exposure leading to allograft rejection

Khodor I. Abou-Daya[1,2], Roger Tieu[1,3], Daqiang Zhao[1,2], Rayan Rammal[4]*, Faruk Sacirbegovic[1,5], Amanda L. Williams[1,2], Warren D. Shlomchik[1,5,6], Martin H. Oberbarnscheidt[1,2,6†], Fadi G. Lakkis[1,2,5,6†]

Copyright © 2021 The Authors, some rights reserved; exclusive licensee American Association for the Advancement of Science. No claim to original U.S. Government Works

Tissue-resident memory T cells (T_{RM}) contained at sites of previous infection provide local protection against reinfection. Whether they form and function in organ transplants where cognate antigen persists is unclear. This is a key question in transplantation as T cells are detected long term in allografts, but it is not known whether they are exhausted or are functional memory T cells. Using a mouse model of kidney transplantation, we showed that antigen-specific and polyclonal effector T cells differentiated in the graft into T_{RM} and subsequently caused allograft rejection. T_{RM} identity was established by surface phenotype, transcriptional profile, and inability to recirculate in parabiosis and retransplantation experiments. Graft T_{RM} proliferated locally, produced interferon-γ upon restimulation, and their in vivo depletion attenuated rejection. The vast majority of antigen-specific and polyclonal T_{RM} lacked phenotypic and transcriptional exhaustion markers. Single-cell analysis of graft T cells early and late after transplantation identified a transcriptional program associated with transition to the tissue-resident state that could serve as a platform for the discovery of therapeutic targets. Thus, recipient effector T cells differentiate into functional graft T_{RM} that maintain rejection locally. Targeting these T_{RM} could improve renal transplant outcomes.

INTRODUCTION

Recent studies have identified noncirculating, memory T cells in nonlymphoid tissues in mice and humans (*1*, *2*). Aptly named tissue-resident memory T cells (T_{RM}), T_{RM} are phenotypically and transcriptionally distinct from circulating effector and central memory T cells and are numerically the largest T cell memory subset in the body (*3*–*5*). T_{RM} form at sites of previous infection outside lymphoid tissues—particularly in barrier organs such as the skin, gut, lungs, and female reproductive tract—and remain there long term, providing local protection against reinfection (*6*–*11*). They have also been observed in cancer (*12*–*14*) and in organs affected by chronic allergy or autoimmunity (*15*–*17*), where they contribute to tumor immunity and tissue pathology.

Despite increasing appreciation of T_{RM} in immunity, their role in organ transplantation is not well understood. Alloreactive effector and memory T cells generated in secondary lymphoid tissues migrate to transplanted organs and are activated and propagate locally to cause rejection (*18*, *19*). In mice and humans, grafts that do not succumb to acute rejection acquire a persistent T cell infiltrate and eventually fail due to chronic rejection (*20*, *21*). Whether T_{RM} form in this setting and contribute to the rejection process is unclear. It has been argued instead that graft T cells become exhausted after repeated exposure to alloantigens (*22*, *23*) and that exhaustion is possibly a mechanism by which grafts are protected from rejection (*24*–*26*). Recent human studies have described donor- and host-derived T_{RM}-like cells in small intestine, lung, and kidney allograft samples based on phenotypic and transcriptional characteristics (*27*–*29*). These studies support the hypothesis that T_{RM} form in organ transplants but do not establish T_{RM} identity based on nonmigratory behavior and do not ascertain their function.

Here, we investigated whether recipient T_{RM} form and function in organ transplants by studying a mouse model in which kidney allografts undergo delayed rejection with chronic features (tubular atrophy, interstitial fibrosis, and vasculopathy) (*21*, *30*, *31*) and monoclonal and polyclonal T cells that infiltrate the graft can be tracked and interrogated over time. This situation differs from previous contexts in which T_{RM} have been commonly studied (e.g., after infection) because the kidney is a nonbarrier, nonmucosal organ and the target foreign antigens persist in abundance alongside the T cells that recognize them (*21*). Using this model, we demonstrated that antigen-specific and polyclonal $CD8^+$ T_{RM} defined by their phenotype, transcriptional profile, noncirculatory behavior, and function do form in allografts, are not exhausted, and cause chronic rejection. Moreover, single-cell analysis of graft T cells early and late after transplantation provided a common atlas of transcriptional programs associated with transition to the tissue-resident state that could serve as a platform for the discovery of therapeutic targets.

RESULTS

Kidney allograft rejection model

To investigate the formation of T_{RM}, we transplanted allogeneic (Balb/c x B6) F1.Act-mOVA (F1.OVA) kidneys, which express chicken ovalbumin (OVA) ubiquitously on cell surfaces, into B6.CD45.1 recipients followed by the adoptive transfer of OVA-specific, $Thy1.1^+$, T cell receptor–transgenic OT-I effector $CD8^+$ T cells 2 days after transplantation (Fig. 1A). In this model, kidney grafts are infiltrated with host, polyclonal T cells that recognize the semiallogeneic graft and monoclonal OT-I cells that recognize the OVA257-264 SIINFEKL peptide in the context of H2-k^b (*21*, *32*).

[1]Thomas E. Starzl Transplantation Institute, University of Pittsburgh School of Medicine, Pittsburgh, PA 15261, USA. [2]Department of Surgery, University of Pittsburgh School of Medicine, Pittsburgh, PA 15261, USA. [3]Medical Scientist Training Program, University of Pittsburgh School of Medicine, Pittsburgh, PA 15261, USA. [4]Division of Anatomic Pathology, Department of Pathology, American University of Beirut, Beirut, Lebanon. [5]Department of Medicine, University of Pittsburgh School of Medicine, Pittsburgh, PA 15261, USA. [6]Department of Immunology, University of Pittsburgh School of Medicine, Pittsburgh, PA 15261, USA.
*Present address: Sloan Kettering Institute, Memorial Sloan Kettering Cancer Center, New York, NY 10065, USA.
†Corresponding author. Email: mho6@pitt.edu (M.H.O.); lakkisf@upmc.edu (F.G.L.)

Downloaded from https://www.science.org at American University of Beirut on April 16, 2024

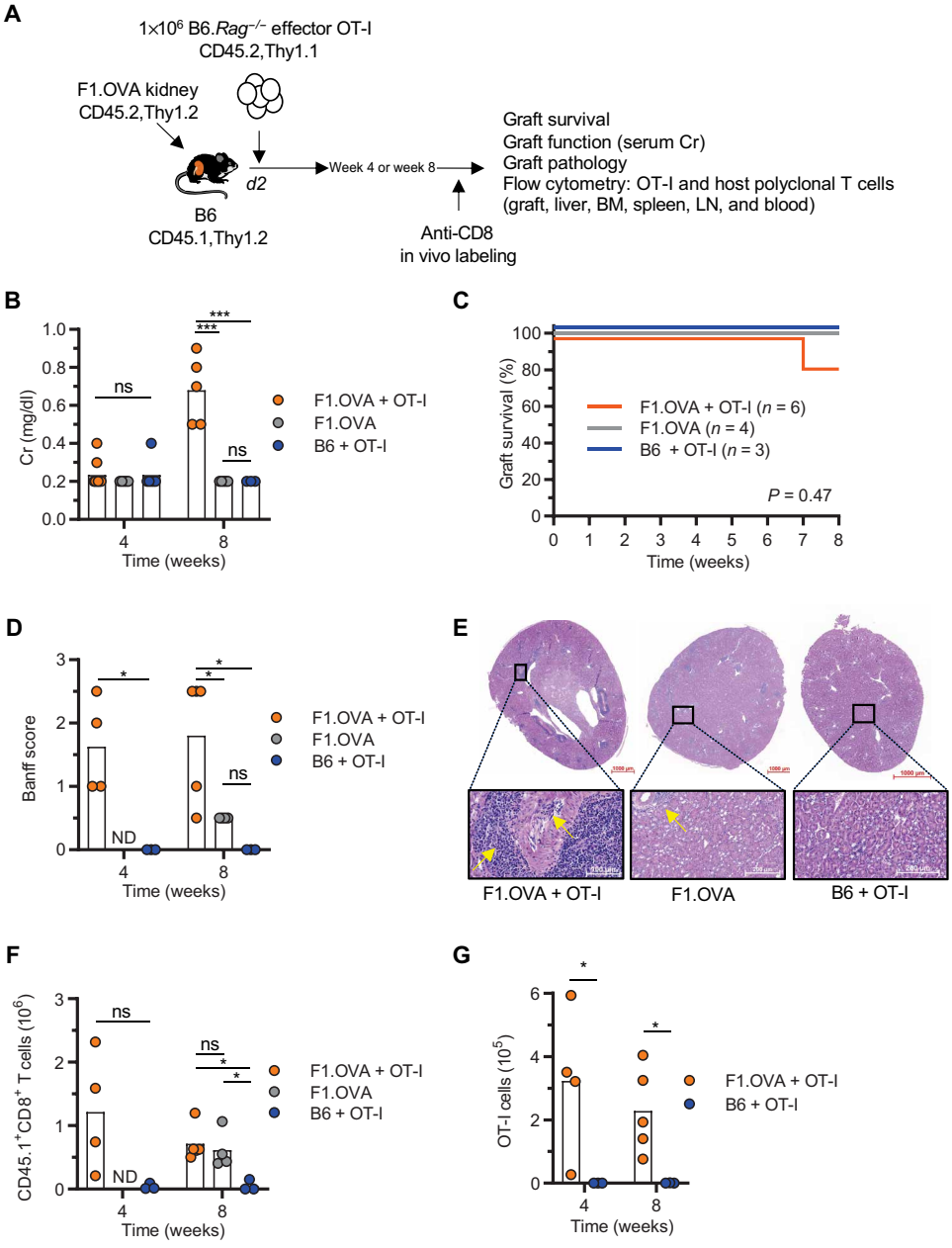

Fig. 1. Chronic kidney allograft rejection model. (**A**) Schematic depicting the mouse kidney transplantation model. (Balb/c x B6)F1.OVA kidney allografts were transplanted to B6 mice that received OT-I effectors (F1.OVA + OT-I group, $n = 4$ to 6 mice, $N = 2$). Control groups consisted of B6 mice that received F1.OVA allografts without OT-I (F1.OVA group, $n = 4$ mice, $N = 2$) or syngeneic grafts with OT-I (B6 + OT-I group, $n = 3$ mice, $N = 1$). LN, lymph node. (**B** to **D**) Graft outcome assessed by serum creatinine (Cr) (B), graft survival (C), and graft pathology score (Banff score) (D). (**E**) Representative micrographs (H&E staining) of graft pathology depicting perivascular cellular infiltrate and vasculitis in the F1.OVA + OT-I group (arrows), mild interstitial inflammation in the F1.OVA group (arrow), and normal histology in the B6 + OT-I group. (**F** and **G**) Quantitation of total host polyclonal $CD8^+$ (F) and monoclonal OT-I (G) T cell infiltrates in the grafts. ND, not done. Individual biological replicates and mean are displayed. One-way analysis of variance (ANOVA) [B, D, and F (week 8)], two-tailed student *t* test [D, F (week 4), and G], and log-rank test (C), $^*P < 0.05$ and $^{***}P < 0.001$. ns, not significant.

The allografts underwent delayed rejection manifesting as graft dysfunction (late rise in serum creatinine with one graft failing at 7 weeks) (Fig. 1, B and C), T cell–mediated graft pathology (Fig. 1, D and E), and infiltration with polyclonal $CD8^+$ and OT-I T cells quantified by flow cytometry at 4 and 8 weeks after transplantation (Fig. 1, F and G). The gating strategy is shown in fig. S1A. In contrast, syngeneic B6 grafts maintained normal function and histology and were not infiltrated with T cells despite the transfer of OT-I effectors to the recipients (Fig. 1, B to G). F1.OVA kidneys transplanted to hosts that did not receive OT-I cells exhibited mild rejection (normal function and borderline pathological changes at 8 weeks), indicating that the transferred OT-I effectors contribute to rejection (Fig. 1, B to G). Therefore, monoclonal OT-I and polyclonal T cells in this model can be tracked over time and their phenotype and function analyzed in the graft.

Graft-infiltrating $CD8^+$ T cells acquired a T_{RM} phenotype

Graft-infiltrating $CD8^+$ T cells were phenotyped by flow cytometry 4 and 8 weeks after transplantation after excluding intravascular $CD8^+$ T cells by in vivo labeling (Fig. 2A). As shown in Fig. 2 (A and B), >80% of host polyclonal $CD8^+$ T cells and virtually all OT-I cells present in the graft had acquired a T_{RM}-like phenotype ($CD44^{hi}CD62L^{lo}CD69^+CD103^{+/-}$) by 4 to 8 weeks. All lacked killer cell lectin-like receptor subfamily G member 1 (KLRG1), which is a marker of short-lived effector T cells, and uniformly expressed CD49a, which is a marker of T_{RM} with cytotoxic functions (Fig. 2A). Although the vast majority of OT-I cells was $CD103^-$, polyclonal $CD8^+$ T_{RM}-like cells contained both $CD103^+$ and $CD103^-$ populations. Donor $CD45.2^+$ $Thy1.2^+CD8^+$ T cells that could have accompanied the graft were extremely rare (Fig. 2A). Treating transplanted mice with cyclosporine, a clinically applicable immunosuppressive agent, did not prevent the formation of OT-I or polyclonal $CD8^+$ T_{RM}-like cells in the graft (fig. S1B).

Graft-infiltrating $CD8^+$ T cells acquired a T_{RM} transcriptional profile

To characterize graft-infiltrating T cells at the transcriptional level, we performed single-cell RNA sequencing (scRNA-seq) on OT-I and polyclonal T cells sorted from kidney allografts early (1 week) and late (5 weeks) after transplantation. Uniform Manifold Approximation and Projection (UMAP) dimensionality reduction of combined week 1 and week 5 OT-I cells demonstrated a homogenous distribution of the cells, with week 1 cells lying predominantly on

Downloaded from https://www.science.org at American University of Beirut on April 16, 2024

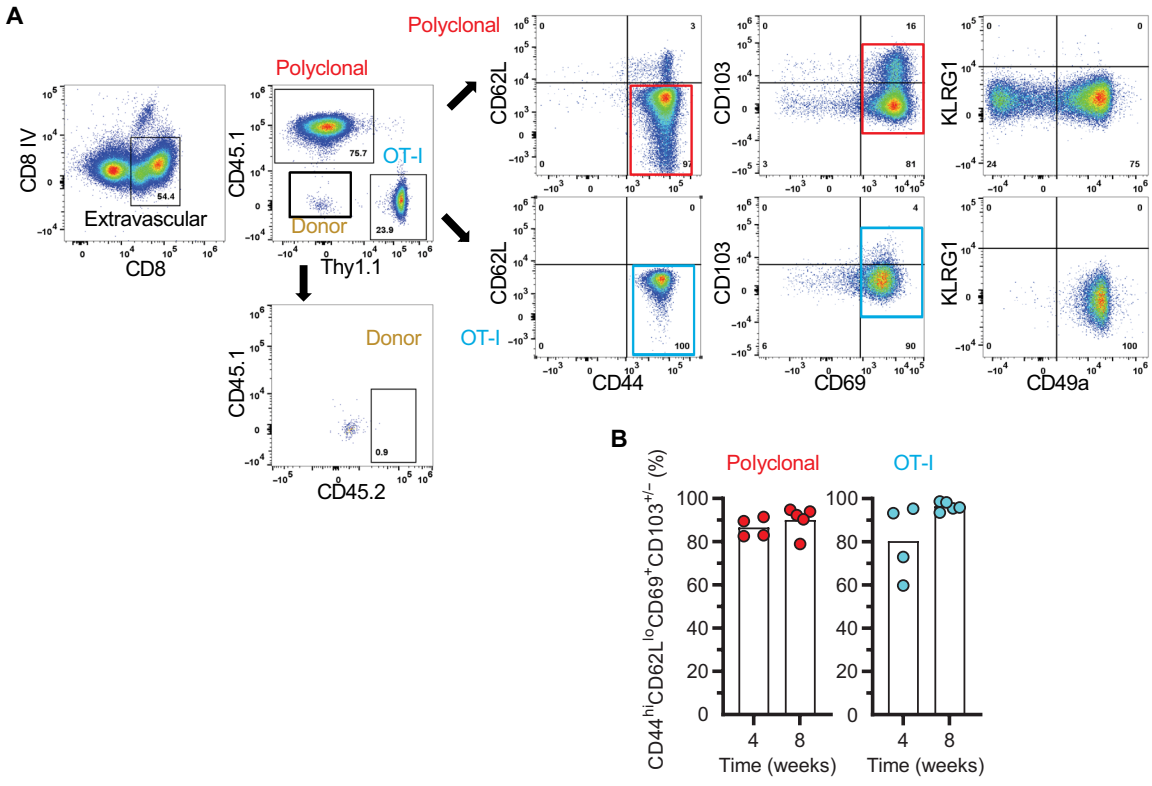

Fig. 2. Graft-infiltrating CD8$^+$ T cells acquired a T_{RM} phenotype. (**A**) Flow cytometry panels depicting the gating strategy to identify and phenotype extravascular, host polyclonal, and OT-I CD8$^+$ T cells in grafts of F1.OVA + OT-I group. A minimal number of donor cells were detected in the graft. Representative of five mice at week 8 and week 4 mice at week 4. (**B**) Proportion of polyclonal and OT-I T cells that acquired a T_{RM} phenotype in the same grafts at week 4 ($n = 4$, $N = 2$) and week 8 ($n = 5$, $N = 2$). Individual biological replicates and mean displayed.

one end of the distribution and week 5 on the other (Fig. 3A). Using *K*-means, we partitioned the OT-I cells into three clusters (Fig. 3A). Week 1 OT-I cells consisted mainly of cluster 1 and week 5 mainly of clusters 2 and 3 (Fig. 3, A and B). Likewise, pseudo-time analysis showed a linear, nonbranching trajectory with progression of cells from week 1 to week 5 and from clusters 1 to 3 (Fig. 3C). Differential gene expression analysis of the three clusters showed increasing up-regulation of T_{RM}-associated transcripts (*Prdm1*, *Nr4a1*, *Nr4a2*, *Rgs1*, *Rgs2*, *Fabp5*, *Bhlhe40*, and *Runx3*) and down-regulation of S1pr1, which is required for T cell egress from tissues (Fig. 3D) (*13*, *33*, *34*). Graft OT-I cells at both week 1 and week 5 scored higher for a memory rather than effector gene signature (fig. S2A) (*35*). Moreover, analysis of batch-effect corrected data combining our dataset with a published circulating OT-I effector scRNA-seq dataset (*36*) showed that all graft OT-I cells occupied a distinct region compared with effectors in UMAP space and have acquired a T_{RM} transcriptional profile as early as the week1 time point (fig. S2B). Therefore, all transferred effector OT-I cells that established residence in the graft adopted a T_{RM} transcriptional profile whose expression increased with time.

Similar analyses were applied to the polyclonal T cell population. UMAP showed a heterogeneous cell distribution, with week 1 cells segregating from week 5 cells (fig. S3A). Multiple T cell subsets in week 5 cells (Fig. 3E) were classified on the basis of their position in UMAP space; *CD8a*, *CD8b1*, *CD4*, and *Foxp3* expression (fig. S3B); and pseudo-time states (fig. S3C). Differential gene expression between CD8$^+$ T cell subsets 1 and 2, which are positioned at opposite ends of the UMAP space (Fig. 3E), uncovered a T_{RM} transcriptional profile in CD8$^+$ T cell subset 2 (Fig. 3F). About 10% of subset 2 consisted of CD4$^+$ T cells, suggesting that it may also contain CD4$^+$ T_{RM}. Ingenuity pathway analysis (IPA) of differentially expressed gene (DEG) showed similar activity of canonical pathways that were common to the OT-I and polyclonal CD8$^+$ T cell subset 2. The top 16 pathways (based on ratio and absolute *z*-score) are shown in Fig. 3G, and the complete list of significant pathways is shown in table S1. Integrin signaling, leukocyte extravasation, actin cytoskeleton signaling, Tec kinase signaling, and RhoA signaling pathways have been previously reported as significant pathways that are common to T_{RM} in a human study that also used IPA analysis (*37*). These scRNA-seq data therefore indicated that all OT-I cells and a subset of polyclonal CD8$^+$ T cells in the graft adopted a transcriptional profile consistent with that of T_{RM}.

Graft-infiltrating CD8$^+$ T cells with T_{RM} phenotype did not recirculate

A defining feature of T_{RM} is their inability to recirculate to other tissues after they form (*38*, *39*). In our model, we found T_{RM}-like OT-I cells only in the kidney allograft—they were absent in host spleen, lymph nodes, blood, bone marrow, and liver—suggesting that they are a nonrecirculating population (Fig. 4A and fig. S4A). To confirm this, we performed a parabiosis experiment in which both parabionts received F1.OVA kidney allografts but only one received OT-I effectors (Fig. 4B). Two to 4 weeks after parabiosis, OT-I cells were present only in the allograft of the mouse that had

Downloaded from https://www.science.org at American University of Beirut on April 16, 2024

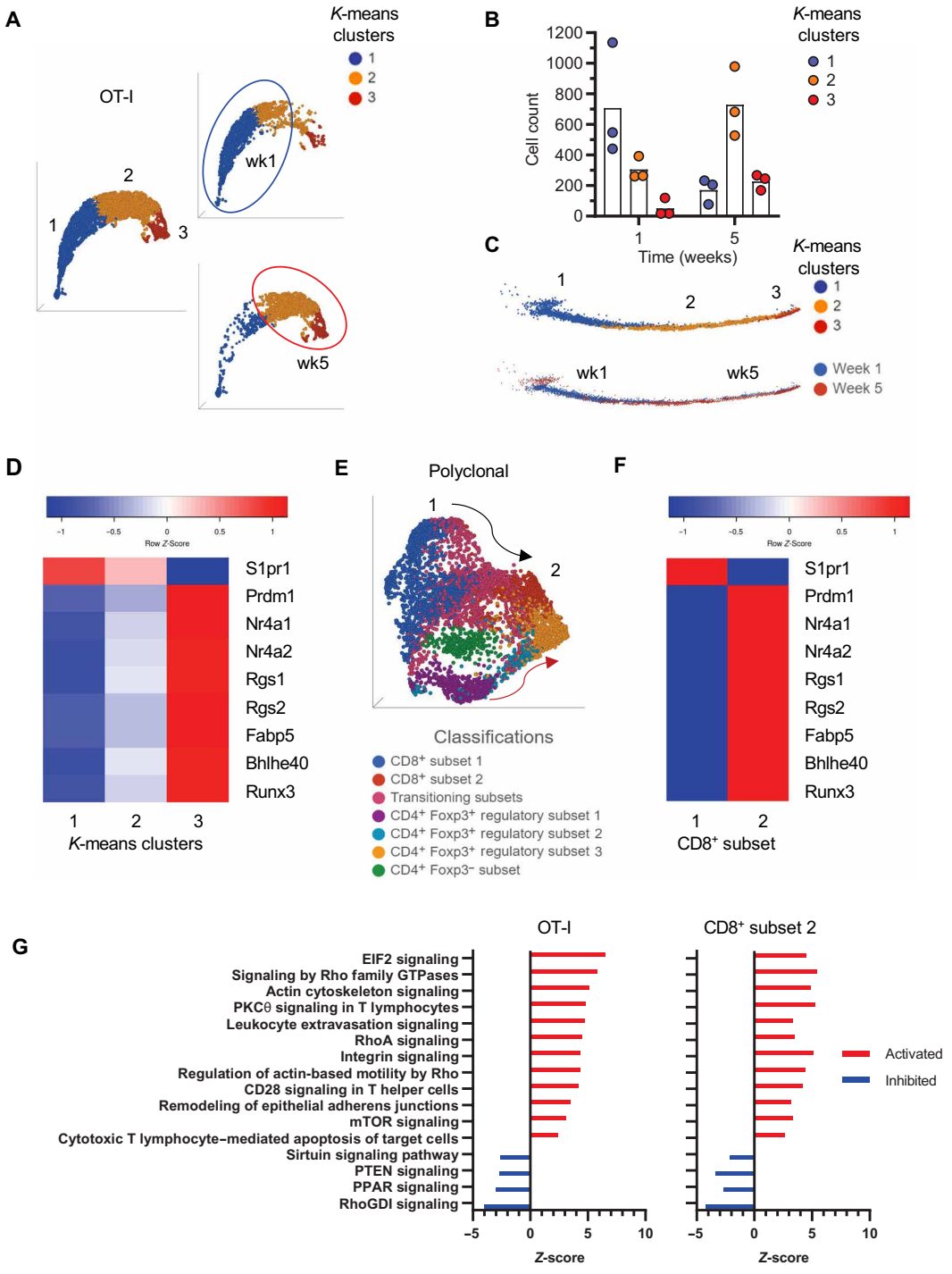

Fig. 3. scRNA-seq analysis of graft-infiltrating CD8$^+$ T cells. (**A**) UMAP and *K*-means clustering of combined week 1 (wk1) and week 5 (wk5) OT-I cells. The right panels highlight projections of wk1 and wk5 cells separately. Circles delineate where the majority of wk1 and wk5 cells is ($n = 3$, $N = 1$ for each time point). (**B**) Scatter plot showing the number of cells in each *K*-means cluster at week 1 and week 5 (individual biological replicates and mean). (**C**) Pseudo-time trajectory inference and *K*-means clustering of combined week 1 and week 5 cells (top trajectory). The bottom trajectory highlights progression from week 1 to week 5 cells in pseudo-time. (**D**) Heatmap of genes associated with T_{RM} phenotype in clusters 1 to 3 depicted in (A) to (C). (**E**) UMAP of week 5 polyclonal T cells classified as shown in fig. S2. The numbers 1 and 2 point to CD8$^+$ subsets at either end of the UMAP space (black arrow). The red arrow highlights the CD4$^+$Foxp3$^+$ trajectory. (**F**) Heatmap of genes associated with T_{RM} phenotype in CD8$^+$ subsets 1 and 2 depicted in (E). (**G**) IPA of DEG in OT-I and CD8$^+$ subset 2 showing similarity in canonical pathway activity between the two cell populations. Top pathways (highest ratio and *z*-score) from table S1 are shown. GTPases, guanosine triphosphatases; PTEN, phosphatase and tensin homolog; PPAR, peroxisome proliferator–activated receptor; EIF2, Eukaryotic Initiation Factor 2.

Downloaded from https://www.science.org at American University of Beirut on April 16, 2024

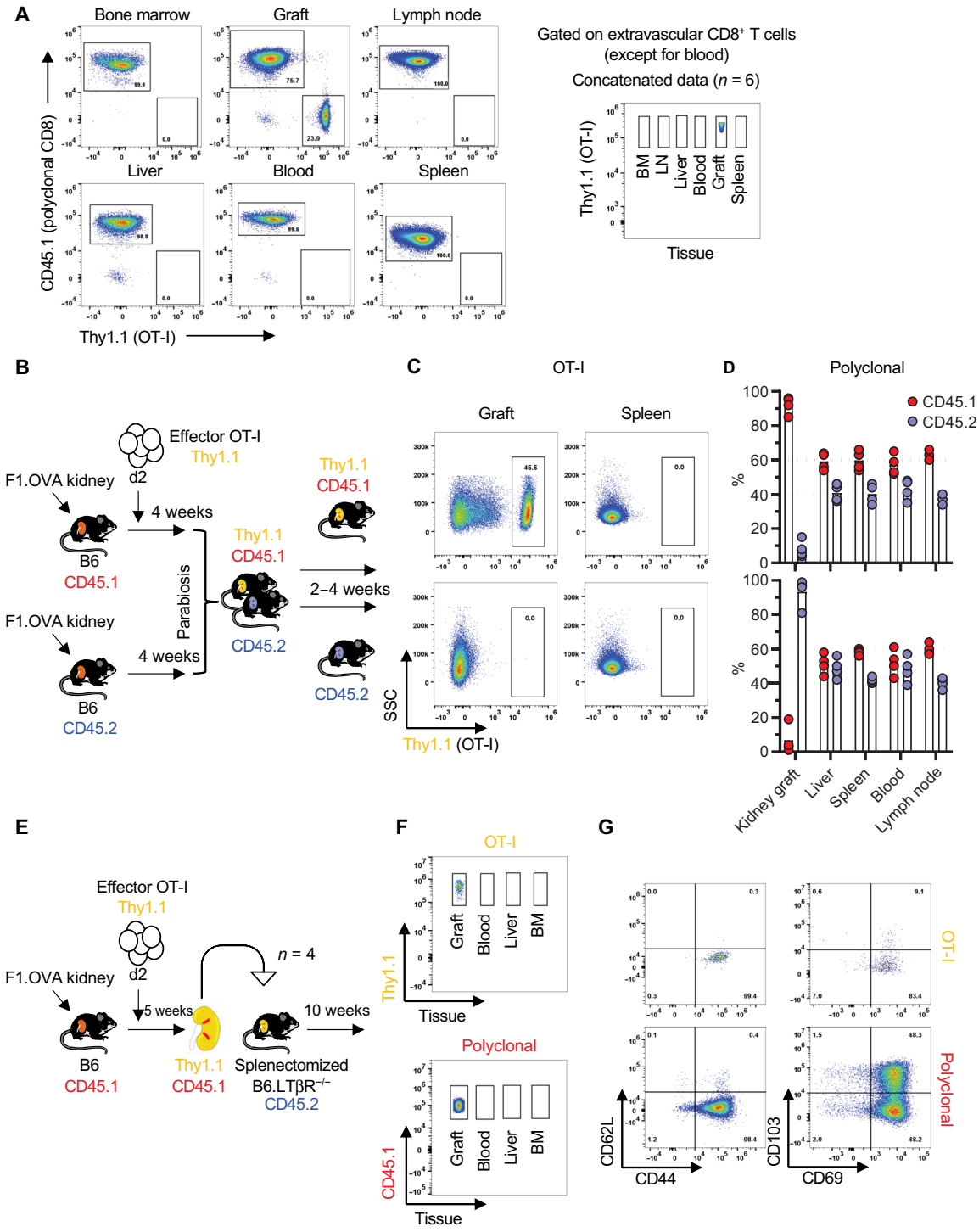

Fig. 4. Graft-infiltrating CD8$^+$ T cells with T_{RM} phenotype did not recirculate. (**A**) OT-I cells at week 8 were present only in the kidney allograft. Representative flow cytometry panels and concatenated data ($n = 6$, $N = 2$) after gating on extravascular CD8$^+$ T cells (except for blood) are shown. BM, bone marrow. (**B** to **D**) Graft OT-I and polyclonal CD8$^+$ T cells did not recirculate after parabiosis. (B) Parabiosis model. (C) Flow cytometry plots of allografts and spleens of parabionts, gating on OT-I cells (rectangles). Representative of $n = 4$ parabiosis pairs, $N = 3$. One pair was harvested at 2 weeks, two pairs at 3 weeks, and one pair at 4 weeks. (D) Cumulative data (individual biological replicates and mean) of polyclonal CD8$^+$ T cells in the grafts and various tissues of parabiosis pairs ($n = 4$, $N = 3$). (**E** to **G**) Graft OT-I and polyclonal CD8$^+$ T cells did not recirculate after kidney allograft retransplantation. (E) Retransplantation model. (F) Concatenated flow cytometry data of graft and other tissues of secondary recipients, gating on OT-I (Thy1.1) and polyclonal CD8$^+$ T cells (CD45.1) of primary recipient ($n = 4$, $N = 1$). (G) Representative flow cytometry plot depicting phenotype of OT-I and polyclonal CD8$^+$ T cells that persist in the graft 10 weeks after retransplantation. Quantification of flow cytometry data in (A), (C), (F), and (G) are shown in fig. S4.

Downloaded from https://www.science.org at American University of Beirut on April 16, 2024

received OT-I effectors but were absent in the graft, spleen, and other tissues of the parabiont (Fig. 4C and fig. S4B). Polyclonal $CD8^+$ T cells from either host equilibrated in the livers, spleens, blood, and lymph nodes of both parabionts, demonstrating that the parabiosis was successful, but did not equilibrate in either kidney graft (Fig. 4D and fig. S5). The latter finding indicated that most of polyclonal $CD8^+$ T cells present in the graft as early as 4 weeks after transplantation were resident. Similarly, both OT-I and polyclonal $CD8^+$ T cells were retained in the graft 10 weeks after retransplantation into hosts that lack secondary lymphoid tissues (Fig. 4, E and F, and fig. S4C). The choice of secondary host [splenectomized lymphotoxin beta receptor deficient ($LT\beta R^{-/-}$)], which does not mount primary immune responses, allowed us to monitor the infiltrate that accompanied the retransplanted grafts over a long period of time. As shown in Fig. 4G and fig. S4D, graft-resident OT-I and polyclonal T cells maintained a T_{RM} phenotype ($CD44^{hi}CD62L^{lo}CD69^+CD103^{+/-}$) 10 weeks after retransplantation. The retransplanted grafts exhibited persistent pathology manifesting as nodular infiltrates, tubulitis, interstitial fibrosis and atrophy, and vasculopathy (fig. S6). Parabiosis and retransplantation experiments therefore established that graft T cells with a T_{RM} phenotype were resident in the graft.

Graft T_{RM} were functional

T_{RM} provide key protection to the host in models of infection and tumor immunity. We therefore asked whether graft T cells shown above to have T_{RM} characteristics (surface phenotype, transcriptional profile, and nonrecirculatory behavior) were also functional. We first found that T_{RM} underwent proliferation in the graft. About 35% of OT-I and 3% of polyclonal $CD8^+$ T_{RM} were 5-bromo-2′-deoxyuridine positive ($BrdU^+$) after 3 days of BrdU administration, and the proportion increased to 100 and 10% after 7 days (Fig. 5A and fig. S7A). Less than 0.5% of either cell population took up 5-ethynyl-2′-deoxyuridine (EdU) after a short (1 hour) pulse, indicating the absence of a significant number of rapidly dividing effector T cells (fig. S7A). We then tested their ability to produce interferon-γ (IFNγ) after restimulation ex vivo. As shown in Fig. 5B and fig. S7B, about 40% of OT-I cells harvested from week 8 grafts were $IFN\gamma^+$ after restimulation with allogeneic cells from the donor. A smaller proportion of polyclonal T cells produced IFNγ (~9%) (Fig. 5B and fig. S7B), consistent with the fact that only a subset of polyclonal cells is alloreactive (*40*, *41*) and only a subset of those differentiated to resident memory (Fig. 2 and Fig. 3). We then investigated whether T_{RM} contributed to rejection by depleting graft OT-I cells with anti-Thy1.1 antibody starting at 4 weeks after transplantation and euthanizing all mice at 8 weeks (Fig. 5C). Specific depletion of OT-I in the graft was confirmed by flow cytometry (Fig. 5, D and E). Eight weeks after transplantation, graft function had deteriorated in untreated mice, whereas it was preserved in depleted mice (Fig. 5F). Graft pathology was similar between the two groups (Fig. 5G). We repeated the same experiment in a separate cohort but monitored the animals for graft survival. As shown in Fig. 5H, renal allografts survival was significantly longer in the

Downloaded from https://www.science.org at American University of Beirut on April 16, 2024

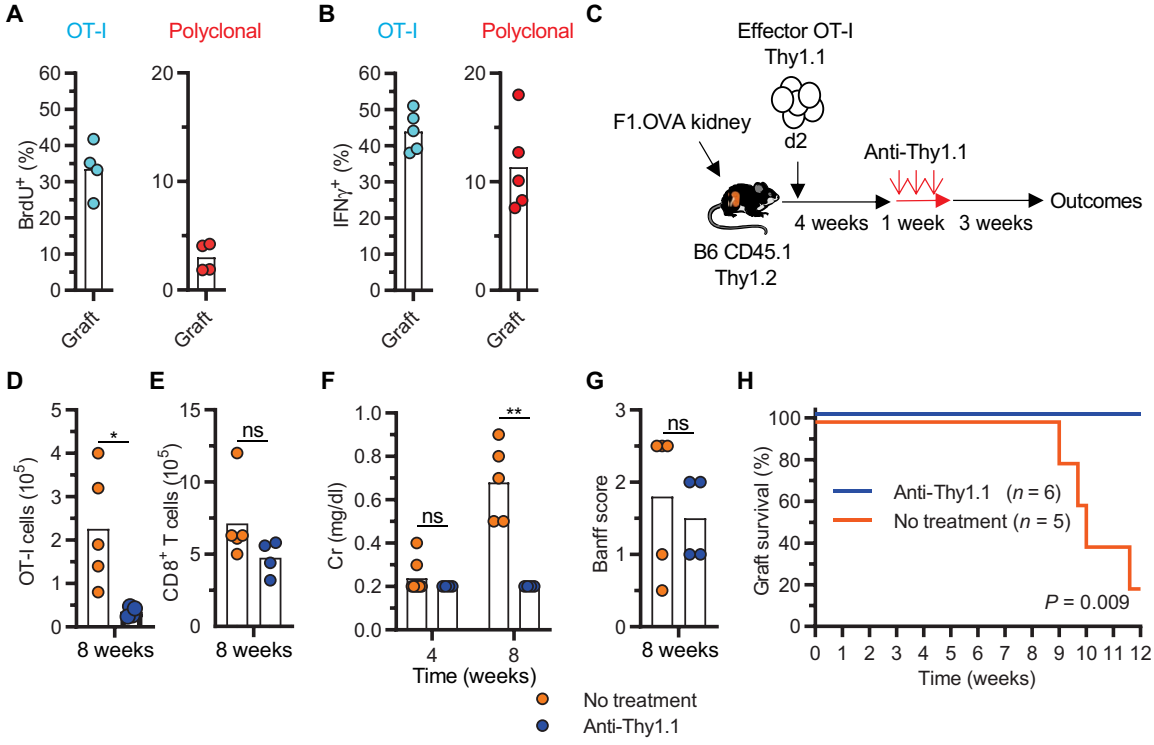

Fig. 5. Graft T_{RM} were functional. (**A**) Proliferation (BrdU uptake) of week 8 graft OT-I and polyclonal $CD8^+$ T cells ($n = 4$, $N = 2$) after 3 days of oral BrdU administration. (**B**) IFNγ production (intracellular staining) by week 8 graft OT-I and polyclonal $CD8^+$ T cells ($n = 5$, $N = 2$) after ex vivo restimulation with allogeneic donor splenocytes. (**C** to **G**) Depletion of graft OT-I cells attenuated graft rejection. (C) Depletion model. (D to G) Quantitation of graft OT-I (D), graft polyclonal $CD8^+$ T cells (E), serum creatinine (F), and graft pathology (G) in nondepleted (no treatment, $n = 5$, $N = 2$) and depleted (anti-Thy1.1, $n = 4$, $N = 1$) groups. Data shown are individual biological replicates and mean. (**H**) Kaplan-Meier curve depicting graft survival after OT-I depletion ($n = 5$ to 6, $N = 1$). Two-tailed Student's *t* test (A, B, D, E, F, and G) and log-rank test (H). $^*P < 0.05$ and $^{**}P < 0.01$.

anti-Thy1.1 group than in the untreated group, indicating that T_{RM} depletion prolonged graft survival in a chronic rejection model.

Lack of exhaustion characteristics in graft T_{RM}

The T_{RM} was characterized in our kidney transplantation model formed in a setting where antigen persisted and where they made contact with antigen-presenting cells (fig. S8). To rule out T cell exhaustion due to persistent antigen (*42*, *43*), we investigated exhaustion markers in both the graft OT-I and polyclonal T_{RM} populations and asked whether treatment with anti–programmed cell death protein-1 (PD-1) accelerates rejection. The majority of OT-I T_{RM} was PD-1^{hi} but lacked all other surface markers of exhaustion [T cell immunoglobulin and mucin domain-containing 3 (TIM-3), lymphocyte-activation gene 3 (LAG-3), and T cell immunoreceptor with Ig and ITIM domains (TIGIT)] (Fig. 6A). Polyclonal T_{RM} had a similar phenotype except for a small minority (~10%) that expressed both PD-1 and TIM-3 but remained LAG-3 and TIGIT negative (Fig. 6A). We also analyzed week 5 scRNA-seq data for enrichment of the exhaustion gene set GSE9650 and compared them with a published scRNA-seq dataset of tumor-infiltrating lymphocytes (TILs) known to harbor exhausted T cells (*35*, *44*). As shown in the histogram (Fig. 6B), exhaustion gene set enrichment in week 5 OT-I and polyclonal T_{RM} was similar to week 1 cells, which are not expected to be exhausted, and conspicuously lower than that in TIL. Specifically, the gene set was enriched in only ~1% of OT-I and ~3% of week 5 polyclonal T_{RM} (Fig. 6C). We then asked whether the resident cells contained progenitors of exhausted T cells defined as PD-1^+TIM3^- TCF1^+, which are a functional cell subset presumably reinvigorated after anti–PD-1 administration (*45*–*47*). As shown in Fig. 6D, only ~2% of OT-I T_{RM} and ~8% of polyclonal $CD8^+$ T cells had this phenotype. However, repeated administration of anti–PD-1 antibody to B6 mice beginning at 30 days after transplanting F1 kidneys failed to precipitate graft rejection or dysfunction, increase total number of polyclonal graft $CD8^+$ T cells, enhance the frequency of either KLRG1$^+$ or KI-67$^+$ $CD8^+$ T cells, or exacerbate graft pathology (fig. S9). Together, these data indicated that the vast majority of graft T_{RM} lacked characteristics of exhaustion.

A common T cell tissue residency program

The polyclonal and OT-I gene datasets generated in the scRNA-seq experiment provided the opportunity to uncover tissue residency programs common to all graft-infiltrating T cells. As previously shown in Fig. 3E and summarized again in Fig. 7A, scRNA-seq analysis of week 5 polyclonal graft T cells, a time point at which resident populations have already been established, identified two trajectories, one for $CD4^+$Foxp3^+ regulatory T cell (T_{reg}) ending in T_{reg} 3, and the other for $CD8^+$ and $CD4^+$ non-T_{regs} ending in the T_{RM} state. T_{reg} 3 and T_{RM} states lay adjacent to each other at the end of their respective trajectories, suggesting a common tissue residency program. To define the genes in this program, we compared the genes that were not differentially expressed between T_{reg} 3 and polyclonal T_{RM} to the DEG of OT-I T_{RM}. The latter was chosen as the reference population to identify the residency program because all the OT-I cells present in the allograft at 5 weeks had become resident (T_{RM}). We found 1204 common genes (Fig. 7A and table S2). IPA of these genes identified significant canonical metabolic, adhesion, and cytokine signaling pathways (Fig. 7B and table S3). Thus, $CD8^+$, $CD4^+$, and T_{reg} subsets that infiltrated the graft shared a common tissue residency program.

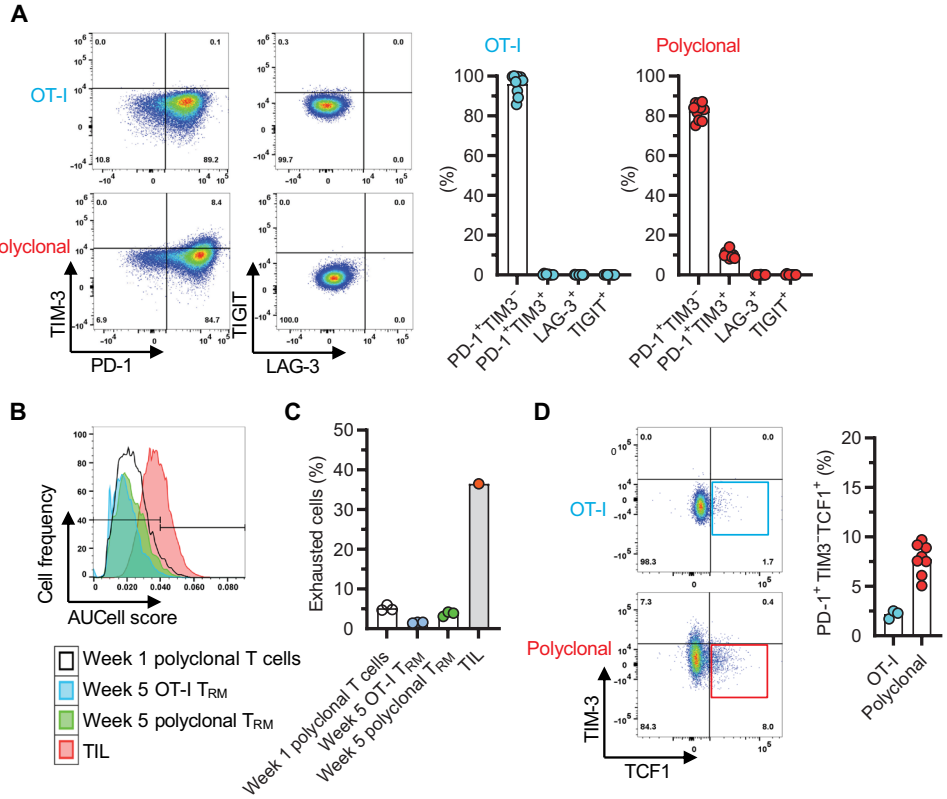

Fig. 6. Lack of exhaustion characteristics in graft T_{RM}. (**A**) Representative flow cytometry panels depicting exhaustion marker expression on graft OT-I and polyclonal $CD8^+$ T cells after gating on the CD44^{hi}CD62L^{lo}CD69$^+$ population 8 weeks after transplantation. Data shown in corresponding bar graphs are individual biological replicates and mean ($n = 10$, $N = 4$). (**B**) Lack of enrichment for the exhaustion gene set (GSE9650) in week 5 graft OT-I and polyclonal T_{RM}. Gene set enrichment was scored on the basis of scRNA-seq data of OT-I and $CD8^+$ subset 2 depicted in Fig. 3. Enrichment of exhaustion gene set in TILs and in week 1 polyclonal graft T cells are included as positive and negative controls, respectively. (**C**) Quantitative representation of data shown in (B), individual biological replicates, and mean [$n = 3$ except for TIL ($n = 1$), $N = 1$]. (**D**) Representative flow cytometry panels showing the proportion of graft OT-I and polyclonal $CD8^+$ T cells that are TIM3$^-$TCF1$^+$ after gating on the CD44^{hi}CD62L^{lo}CD69$^+$PD-1$^+$ population at 4 to 10 weeks after transplantation. Data are individual biological replicates and means ($n = 3$ and $N = 2$ for OT-I and $n = 8$ and $N = 3$ for polyclonal).

DISCUSSION

Here, we demonstrated that $CD8^+$ T_{RM} defined by their phenotype, transcriptional profile, noncirculatory behavior, and function form in allografts and contribute to chronic rejection. Only a minority of these cells displayed exhaustion characteristics. Moreover, antigen-specific

Downloaded from https://www.science.org at American University of Beirut on April 16, 2024

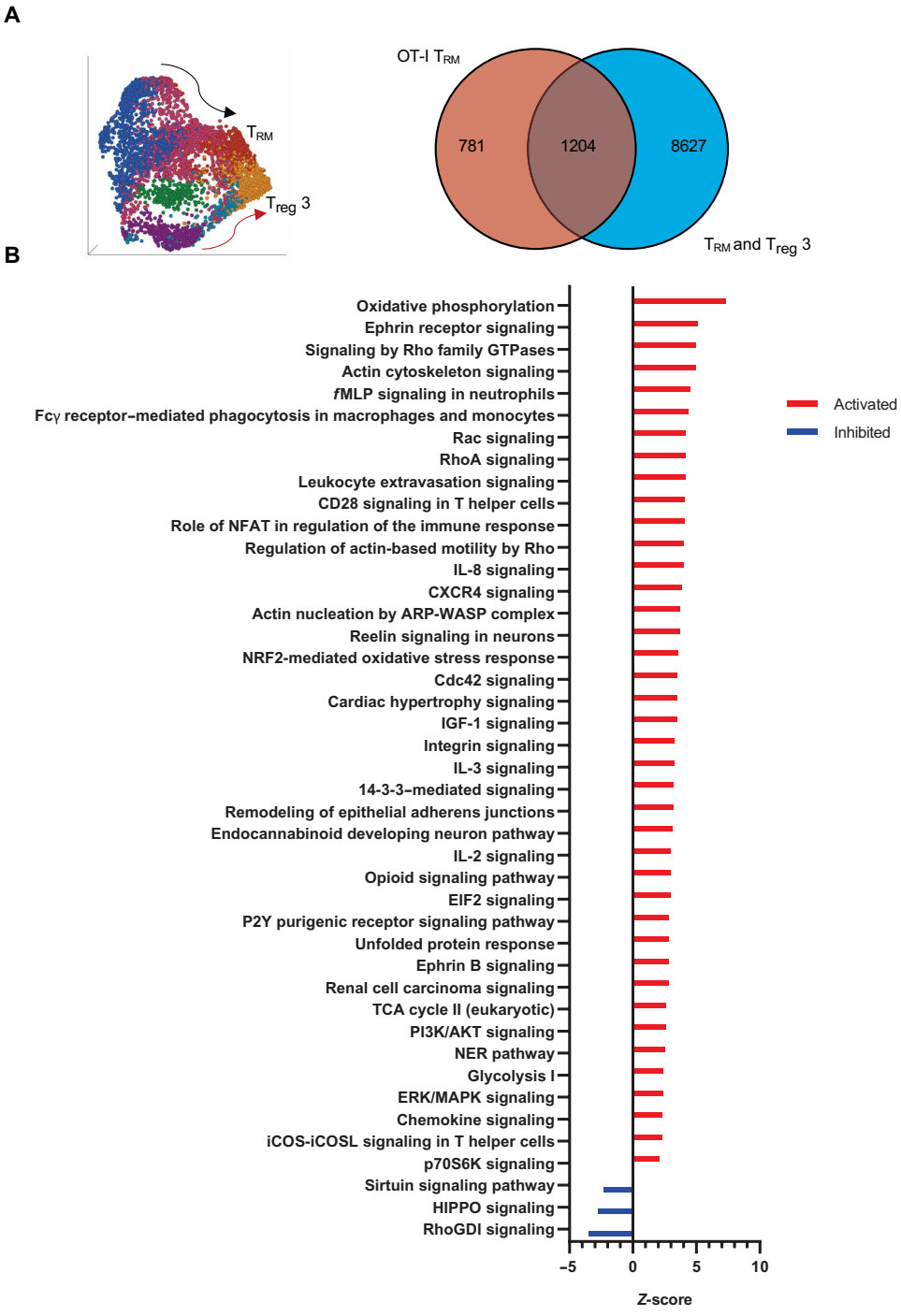

Fig. 7. A common T cell tissue residency program. (**A**) Venn diagram illustrating the number of genes shared between DEG of OT-I T_{RM} and non-DEG of polyclonal T_{RM} and $CD4^+Foxp3^+$ regulatory subset 3 (T_{reg} 3) depicted in UMAP on left and in Fig. 3E. (**B**) IPA of the shared gene set. Pathways listed were identified as significant based on −log(BH *P* value) > 1.3, ratio > 0.1, *z*-score > [2]. *f*MLP, *N*-formyl-Met-Leu-Phe; NFAT, nuclear factor of activated T cells; IL-8, interleukin-8; IGF-1, insulin-like growth factor 1; PI3K, phosphatidylinositol 3-kinase; NER, nucleotide excision repair; ERK, extracellular signal–regulated kinase; MAPK, mitogen-activated protein kinase; ARP, actin-related protein complex; WASP, Wiskott-Aldrich syndrome protein; NRF2, nuclear factor erythroid 2–related factor 2; iCOS, inducible T Cell costimulator; iCOSL, inducible T cell costimulator ligand.

$CD8^+$ T_{RM} shared a transcriptional tissue residency program with other graft-infiltrating T cells. Our findings extend the concept of T_{RM} to settings such as transplanted allografts where foreign antigens persist in abundance. They also provide insights into combating chronic rejection, a recalcitrant problem in organ transplant recipients.

Our results are supported by earlier data suggesting the presence of T_{RM} in organ transplants. Hadley and colleagues (*48*–*51*) described $CD103^+$ T cells in rodent islet and kidney allografts and showed that depleting these cells ameliorates rejection. However, the authors did not determine whether $CD103^+$ T cells were resident and instead assumed that they were recently migrated effector T cells with affinity to epithelial cells due to CD103 expression. In humans, one study demonstrated that recipient, alloreactive T cells with a T_{RM} phenotype establish residence in small bowel allografts and acquire an activation phenotype during rejection episodes (*27*). Another identified donor and recipient T_{RM} in lung allografts and provided evidence that persistence of donor T_{RM} correlates with fewer adverse clinical events (*28*). Unlike human allografts, we did not observe any significant donor T_{RM} in mouse kidney transplants. This difference may be ascribed to paucity of resident lymphocytes in native organs of specific pathogen free (SPF) animals (*52*) or the fact that human transplant recipients receive chronic immunosuppression that prevents the rejection of donor leukocytes that accompany the graft. The results of our study established the presence of T_{RM} in organ transplants beyond what could be gleaned from human samples by definitively demonstrating that they are nonrecirculatory and that they function in situ.

The observation that bona fide T_{RM} formed in the allograft implied that persistent antigen did not preclude the formation of T_{RM}. This puts our model on par with descriptions of T_{RM} in tumors and autoimmune disease (*13*, *16*) but distinguishes it from classical models of infection in which T_{RM} were observed after antigen clearance. Whether T_{RM} continually contact cognate antigen in the graft was not fully ascertained in this study, although we did provide evidence that a substantial proportion of antigen-specific T_{RM} were contacting graft dendritic cells in a stable fashion. This is consistent with our previous work showing that recently migrated effector/memory T cells make frequent cognate interactions with the dense network of dendritic cells found in kidney

Downloaded from https://www.science.org at American University of Beirut on April 16, 2024

tissue, especially in the presence of ubiquitously expressed antigen (e.g., OVA) (*21*, *53*). However, unlike tumor models (*42*, *44*, *54*), we did not detect significant evidence of exhaustion in graft T_{RM} and were unable to exacerbate renal allograft rejection with delayed administration of an anti–PD-1 antibody known to enhance tumor immunity (*44*, *55*). Although a prior study showed that checkpoint blockade increases mouse renal allograft pathology, the investigators could only elicit this effect if the antibody was administered very early after transplantation (*56*). Therefore, it is possible that the graft microenvironment lacks the conditions present in the tumor microenvironment that have been associated with chronic T cell dysfunction. These include competition for glucose, low pH, and accumulation of lactic acid (*44*). Alternatively, the transforming growth factor–β–rich cytokine milieu in the allograft may favor T_{RM} formation as has been shown in other tissues (*57*, *58*).

The presence of functional T_{RM} in the allograft is of high clinical significance because chronic rejection remains a major obstacle to long-term allograft survival. Systemic immunosuppression has not succeeded in halting chronic rejection possibly because it targets the more readily accessible circulating naïve and memory T cells but fails to suppress T cells in the graft. Therefore, dissecting the biology of T_{RM} in the setting of transplantation could shed light on ways to eliminate T_{RM} and subsequently improve transplantation outcomes.

MATERIALS AND METHODS

Study design

We developed a mouse kidney transplantation model to study the role of T_{RM} in transplantation. Three biological replicates (three individual transplant recipients) per group were included in each experiment. Both sexes of mice were used, but male mice proved to be more suitable for the transplantation procedure due to size and anatomy. Donor-recipient pairs were sex matched. Experiments were repeated once in most instances, resulting in a total of up to six biological replicates. scRNA-seq experiment was only performed once with three biological replicates per group. Sample sizes were not based on power analysis but on our prior experience that three to six biological replicates were sufficient to discern statistically significant differences between groups using the same readout (number of tissue-resident T cells) (*21*). Sample size was not altered at any time during the course of the study. A biological replicate was excluded only if the mouse died within the first 7 days after transplantation, which was considered a technical failure. This exclusion criterion was established prospectively, it occurred very rarely, and we did not experience any technical problems in harvesting or analyzing the grafts that would have led to exclusion of a biological replicate. All data points were included, and no outliers were excluded. All end points were prospectively selected. It was not possible to blind the study because of the need to identify donors and recipients and because, in many instances, the donor or recipient groups had different coat colors. The first investigator (K.I.A.-D. or R.T.) to analyze the flow cytometry data was not blinded, but randomly chosen subset of groups were reanalyzed blindly by either M.H.O. or F.G.L. Histological interpretation of tissue sections was performed blinded by R.R.

Mice

B6.CD45.2 (C57BL/6J; Thy1.2, CD45.2), B6.CD45.1 (B6.SJL-Ptprc^a Pepc^b/BoyJ, Thy1.2, CD45.1), B6.CD11c-YFP [B6.Cg-Tg(Itgax-Venus)1Mnz/J], and DsRed [B6.Cg-Tg(CAG-DsRed*MST) 1Nagy/J] were purchased from the Jackson Laboratory (Jax) and B6.CD45.1 (B6.SJL-Ptprc^{a}Pepc^b/BoyCrCrl) from Charles River Laboratories. OT-I mice (C57BL/6-Tg[TcraTcrb]1100Mjb/J; CD45.2) were obtained from Jax and maintained on a Rag$^{-/-}$ Thy1.1 or Rag$^{-/-}$ DsRed background. F1.OVA mice were generated by breeding BALB/cJ mice with B6.*Act-OVA (C57BL/6-Tg(CAG-OVAL)-916Jen/J)*. B6.ltbr$^{-/-}$ mice were obtained from Y.-X. Fu (previously at the University of Chicago) and maintained at the University of Pittsburgh animal facility. Mice were maintained under SPF conditions. Both male and female mice were used except that female recipients were avoided because of surgical constraints. All mouse work was performed in compliance with ethical regulations and was approved by the Institutional Animal Care and Use Committee of the University of Pittsburgh.

Antibodies and reagents

All antibodies used for flow cytometry are listed in table S4. Antibodies used for in vivo administration were anti-mouse Thy1.1 monoclonal antibody (mAb) (19E12, Bio X Cell), rat anti-mouse PD-1 (29F.1A12, Leinco Technologies), and rat immunoglobulin G2a (IgG2a) isotype control (1-1, Leinco Technologies).

From Sigma-Aldrich, we obtained Ficoll-Paque PREMIUM 1.084, collagenase IV, deoxyribonuclease I (DNAse I), and collagenase IV. From Cedarlane, we obtained lympholyte M. Dec205-OVA fusion antibody was provided by the laboratory of W.D.S. at the University of Pittsburgh. Anti-CD40 (FGK45) was purchased from Bio X Cell.

Surgical procedures

Mouse kidney transplants were performed as previously described (*53*) using (BALB/c x B6)F1.*mAct-OVA*, (BALB/c x B6)F1, or B6 donors and B6 recipients. Recipient native kidneys were removed at the time of transplantation. Allograft rejection was monitored by visual observation of recipients for signs of uremia (lethargy, decreased mobility, and ruffled hair) or death. Allograft function was monitored by serial serum creatinine measurements using an i-Stat Analyzer (Abbott) at a lower detection limit of 0.2 mg/dl. For kidney retransplantation, the kidney graft from the primary recipient was harvested along with the ureter, renal vein, renal artery, abdominal aorta, and inferior vena cava. The primary recipient's aorta was then anastomosed end to side to the secondary recipient's aorta, followed by end-to-side anastomosis of the inferior venae cavae. The ureter was implanted into the posterior wall of the secondary recipient's bladder of and the recipient then underwent bilateral nephrectomy. Parabiosis was performed as described previously (*59*). Briefly, age-, size-, and gender-matched transplanted recipients were anesthetized and a longitudinal skin incision made from elbow to knee joint. Elbow and knee joints were attached using surgical nonabsorbable sutures, and skin was closed in the ventral and dorsal areas. Splenectomy was performed as previously described (*18*). Mice received antibiotic chow for 10 days after surgery.

Mouse treatment

To assess in vivo cell proliferation, mice received 1 mg of EdU (Bio Legend) intraperitoneally 1 hour before euthanasia and BrdU (Life Technologies) in the drinking water (1 mg/ml) for either 3 or 7 days before euthanasia. To deplete T_{RM}, 250 μg of anti-Thy1.1 mAb (Bio X Cell) was administered intravenously daily for 7 days. Anti–PD-1

Downloaded from https://www.science.org at American University of Beirut on April 16, 2024

mAb (clone 29 F.1A12 obtained from D. Vignali, University of Pittsburgh) or isotype control antibody (IgG2a, Bio X Cell) was administered intraperitoneally (200 μg per dose every 3 days) as shown in fig. S5A. Cyclosporine (Sigma-Aldrich) immunosuppression was given subcutaneously (250 μg per dose) daily for 14 days.

Generation and adoptive transfer of OT-I effector T cells

B6.Rag$^{-/-}$ OT-I DsRed^{+} or Thy1.1^{+} (CD45.2) (1×10^5 to 6×10^5) splenocytes were transferred intravenously to B6 (CD45.1) mice. Mice were then injected with 25 μg of anti–Dec205-OVA antibody (Dec205-OVA) intravenously plus 50 μg of agonistic anti-CD40 (FGK45) intraperitoneally to generate OT-1 effector cells (*60*). Spleens were harvested 5 days later, and CD45.2^{+}DsRed^{+}/Thy1.1^{+} CD4^{-}CD45.1^{-} Lin (CD11c, CD11b, Ter119, CD16/32, B220, F4/80, and DX5)$^{-}$ cells were sorted on a high-speed cell sorter (BD FACSAria). Sorted cells were washed and counted, and 1×10^6 cells were injected intravenously into transplanted mice. The vast majority of transferred OT-I cells was CD44^{hi}CD62L^{lo} (*61*).

Tissue digestion and flow cytometry

Before organ procurement, mice were anesthetized and then intravenously injected with 3 μg of anti–CD8a-eFluor450 antibody 2 min before euthanasia to label blood-localized cells (*62*). The kidney graft, spleen, inguinal and mesenteric lymph nodes, bone marrow, blood, and liver were procured. Kidney grafts and livers were homogenized using a gentleMACS tissue homogenizer (Miltenyi Biotec) and then incubated in RPMI 1640 media containing collagenase IV (350 U/ml), DNAse I (0.02 mg/ml), and 5% fetal bovine serum for 60 min at 37°C. Single-cell suspensions were filtered through a 40-μm filter and washed. Spleens and lymph nodes were homogenized by crushing them through a 40-μm filter. Red blood cell (RBC) lysis was performed on blood, bone marrow, and spleen single-cell suspensions for 5 min at room temperature using an RBC lysis buffer (Sigma-Aldrich). Cells were then stained for viability and cell surface markers and analyzed by flow cytometry (BD LSRFortessa or Cytek Aurora). Intracellular staining for IFNγ was performed 16 hours after ex vivo stimulation with donor splenocytes and analyzed by flow cytometry as previously described (*63*). BrdU and EdU staining were performed according to the manufacturer's protocols (Phase-Flow Alexa Fluor 647 BrdU Kit, BioLegend, using anti–BrdU–Alexa Fluor 647 mAb, clone MoBU-1, Life Technologies; EdU Click-iT Plus EdU Alexa Fluor 488 Flow Cytometry Assay Kit, Life Technologies). Fluorescence minus one controls were prepared for each antibody to define positive gates.

Histological analysis

Kidney allograft tissue was fixed in paraformaldehyde, paraffin-embedded, sectioned, and stained with hematoxylin and eosin (H&E), Masson trichrome, periodic acid–Schiff, and Verhoeff–Van Giessen stain using the Magee-Womens Research Institute Histology and Microimaging Core, University of Pittsburgh. All slides were scanned on a Zeiss Axioscan (Zen v2.3) with a 20× objective [Plan-Apochromat 20×/0.8 WD (working distance) = 0.55], read blindly by a renal pathologist (R.R.), and graded according to the Banff criteria (*64*). Briefly, extent of tubular, interstitial, vascular, and glomerular infiltrate was scored to determine the Banff grade. Banff grades were assigned numerical values: normal = 0, borderline = 0.5, IA = 1.0, IB = 1.5, IIA = 2.0, and IIB = 2.5.

Two-photon intravital imaging

Multiphoton intravital microscopy was performed on transplanted kidneys. A custom Leica TCS SP8 Triple Beam 6 Ch NDD system containing six HyD (hybrid detector) detectors and two Spectra Physics femtosecond pulsed lasers (Mai Tai DeepSee and Insight X3) with three laser lines was used. The laser was tuned and mode locked to 920 nm. The following filter sets were used: Ch1 (583/22) (dsRed), Ch2 (537/26)(EYFP), and Ch5 (655/15)(Evans Blue). Microscope data were acquired with Leica LAS X v2.53. Mice were anesthetized with isoflurane and oxygen and core body temperature maintained at 37°C with a homeothermic controller (TC-1000, CWE, Ardmore, PA). Animals were kept hydrated by injecting 1 ml of 5% dextrose lactated Ringer's solution subcutaneously every 60 min. Blood vessels were visualized by injecting Evans Blue [3 to 6 μl of stock solution (5 mg/ml; 15 to 30 μg) diluted in phosphate-buffered saline intravenously]. The kidney graft was extraverted from the abdominal cavity with intact vascular connection and immobilized in a custom cup mount (*65*). A coverslip was placed on top of the kidney, and *z*-stacks were visualized with a 25× water immersion objective (numerical aperture, 1.05) up to 50 μm below the kidney capsule. All stacks were acquired with a step size of 1 μm. Brightness and laser power were adjusted on the basis of the imaging depth and kept below phototoxic levels. Line averaging was set to 3× at a resolution of 512 by 512 pixel using the resonance scanner. Time-lapse imaging was performed for ~30 min per location. Up to five different locations per kidney graft were imaged. All acquired movies were analyzed using Imaris software V9 (Bitplane). Drift was corrected using dendritic cells as a reference point. Background subtraction was performed on all channels equally. OT-I–dendritic cell contacts were quantitated using the Imaris kiss-and-run plugin with a threshold of 2 μm and a minimal duration of 2 min.

Bioinformatics analyses

Dimensionality reduction was performed using UMAP with the following parameters: local neighborhood size = 15, minimal distance = 0.1, distance metric = Euclidean, initialization = random, and number of principal components = 5. By visualizing cells in three dimensions based on their gene expression, UMAP allowed for the gross description of gene expression patterns and detection of cell neighborhoods. To demonstrate the temporal states of gene expression in cell populations, pseudo-time trajectory inference (monocle 2) was used. In the case of the OT-I cell population, *K*-means clustering algorithm was used to partition the cells into three clusters (max iterations = 1,000,000) representing three time points along the nonbranching pseudo-time trajectory. Gene expression (LSMean) of clusters or states was visualized in heatmaps generated by Heatmapper (*66*). DEG lists of OT-I T_{RM} were determined by performing analysis of variance (ANOVA) on gene expression of OT-I clusters. The results were filtered as follows: false discovery rate (FDR) < 0.01 in all contrasts, cluster 3 versus 1 (fold change, >2 and <−2), cluster 2 versus 1 (fold change, >1 or <−1), and cluster 3 versus 2 (fold change, >1 or <−1), and LSMean > 1000 to exclude low expressed genes and limit gene numbers to ~2000 for downstream analysis. A similar approach was used to obtain the DEG of polyclonal T_{RM} in the comparison between CD8^{+} subset 2 versus 1 (FDR < 0.01; fold change, >2 and <−2; LSMean > 500). Polyclonal T_{RM} non-DEGs between polyclonal T_{RM} and T_{reg} 3 were identified by setting the FDR at >0.01 and fold change at <2 and >−2. IPA (QIAGEN) was performed to identify significant canonical

Downloaded from https://www.science.org at American University of Beirut on April 16, 2024

pathways [–log(Benjamini-Hochberg *P* value) > 1.3, ratio > 0.1, and *z*-score > [2]). Top pathways were identified by selecting highest ratio and *z*-score pathways with exclusion of ubiquitous pathways (such as oxidative phosphorylation). Cells were rank scored for enrichment of the exhaustion gene set GSE9650 using AUCell. Exhaustion scores from AUCell were visualized and analyzed using FlowJo v10.6.0 (BD).

Cell preparation and sorting of scRNA-seq

F1.OVA kidney allografts were harvested 1 or 5 weeks ($n = 3$ from each time point) after transplantation from recipients that also received 1×10^6 effector DsRed$^+$ OT-I cells on day 2 (fig. S10). In vivo labeling was performed using 3 μg of anti-CD45 intravenously 2 min before euthanasia. Lin$^-$(CD11c, CD11b, Ter119, CD16/32, B220, F4/80, DX5, NK1.1, Ly6g, and CD19) and intravascular CD45$^+$ cells were excluded from sorted cell population. Polyclonal CD45.1$^+$dsRed$^-$Thy1.2$^+$CD5$^+$ T cells and monoclonal CD45.1$^-$ dsRed$^+$Thy1.2$^+$CD5$^+$ OT-I cells were sorted separately from each harvested graft. Each sorted polyclonal and OT-I T cell sample was then labeled with cell-hashing antibodies (TotalSeq-A, BioLegend) (table S4) for later demultiplexing (*67*). Polyclonal and OT-I T cell samples were pooled separately and sequenced.

scRNA-seq and data preprocessing

scRNA-seq was performed using 10X Genomics Single Cell 3′ kit, version 2, according to the manufacturer's instructions, with 7000 sorted polyclonal or OT-I T cells loaded for each sample. mRNA and hashtag oligos cDNA libraries from pooled samples were sequenced on the NextSeq500 Platform (Illumina). Raw fastq files were preprocessed and analyzed using Partek Flow v9.0.20.0110 (Partek) default setting unless otherwise stated. Alignment to the mm10 mouse genome, filtering, barcode and unique molecular identifier counting and deduplication, low-quality cell filtration, batch-effect removal, and hashtag demultiplexing were applied as recommended in Partek Flow. Multiplets and cells with greater than 3% mitochondrial gene expression were excluded, resulting in a gene expression matrix of 6580 cells by 12,318 genes (OT-I) and 11700 cells by 15,293 genes (polyclonal). Data were normalized by $\log_2$(counts per million + 1). TIL data were downloaded from Gene Expression Omnibus (GEO; https://ncbi.nlm.nih.gov/geo/) using accession codes GSE122675 and then normalized similar to the data from the graft-infiltrating cells (*44*). Exhaustion gene set GSE9650 EXHAUSTED VS MEMORY CD8 TCELL UP (Exhaustion Gene Set), EFFECTOR VS MEMORY CD8 TCELL DN (Memory Signature), and EFFECTOR VS MEMORY CD8 TCELL UP (Effector Signature) were downloaded from Molecular Signatures Database v7.0 (https://gsea-msigdb.org/gsea/msigdb/index.jsp) (*35*). See Supplementary Methods for bioinformatic analyses.

Statistics

Statistical analysis of allograft survival was calculated using the log-rank test. All other experiments were analyzed using two-tailed, nonparametric, unpaired *t* test or one-way ANOVA with Tukey's multiple comparison. All statistical calculations were made using GraphPad Prism version 9.0.0. A $P < 0.05$ was considered significant. All data points are shown in the graphs as scatterplots with mean value indicated by a horizontal bar. All statistical analyses were $^*P < 0.05$, $^{**}P < 0.01$, $^{***}P < 0.0001$, and $^{****}P < 0.0001$; ns indicates not significant.

SUPPLEMENTARY MATERIALS

immunology.sciencemag.org/cgi/content/full/6/57/eabc8122/DC1
Fig. S1. Gating strategy to identify graft-infiltrating CD8$^+$ and OT-I cells.
Fig. S2. Transcriptomic comparison among OT-I populations.
Fig. S3. scRNA-seq analysis of graft polyclonal T cells—classification strategy.
Fig. S4. Quantitation of flow cytometry data from Fig. 4.
Fig. S5. Distribution of polyclonal CD8$^+$ T cells in tissues and allografts of parabionts.
Fig. S6. Representative pathology in retransplanted kidneys.
Fig. S7. Proliferation and IFNγ production in graft OT-I and polyclonal CD8$^+$ T_{RM}.
Fig. S8. Intravital two-photon microscopy of F1.OVA kidney graft.
Fig. S9. Anti–PD-1 treatment does not enhance rejection.
Fig. S10. Flow cytometry sorting strategy of graft OT-I and polyclonal T cells for scRNA-seq.
Table S1. Canonical pathways in OT-I T_{RM} (Excel spreadsheet).
Table S2. Common tissue residency associated genes (Excel spreadsheet).
Table S3. Canonical pathways associated with tissue residency (Excel spreadsheet).
Table S4. Antibody list (Excel spreadsheet).
Table S5. Raw data file (Excel spreadsheet).

View/request a protocol for this paper from *Bio-protocol*.

REFERENCES AND NOTES

1. D. Masopust, A. G. Soerens, Tissue-resident T cells and other resident leukocytes. *Annu. Rev. Immunol.* **37**, 521–546 (2019).
2. M. E. Snyder, D. L. Farber, Human lung tissue resident memory T cells in health and disease. *Curr. Opin. Immunol.* **59**, 101–108 (2019).
3. D. Masopust, V. Vezys, A. L. Marzo, L. Lefrancois, Preferential localization of effector memory cells in nonlymphoid tissue. *Science* **291**, 2413–2417 (2001).
4. R. A. Clark, B. Chong, N. Mirchandani, N. K. Brinster, K. I. Yamanaka, R. K. Dowgiert, T. S. Kupper, The vast majority of CLA$^+$ T cells are resident in normal skin. *J. Immunol.* **176**, 4431–4439 (2006).
5. J. J. Milner, A. W. Goldrath, Transcriptional programming of tissue-resident memory CD8$^+$ T cells. *Curr. Opin. Immunol.* **51**, 162–169 (2018).
6. T. Gebhardt, L. M. Wakim, L. Eidsmo, P. C. Reading, W. R. Heath, F. R. Carbone, Memory T cells in nonlymphoid tissue that provide enhanced local immunity during infection with herpes simplex virus. *Nat. Immunol.* **10**, 524–530 (2009).
7. X. Jiang, R. A. Clark, L. Liu, A. J. Wagers, R. C. Fuhlbrigge, T. S. Kupper, Skin infection generates non-migratory memory CD8$^+$ T_{RM} cells providing global skin immunity. *Nature* **483**, 227–231 (2012).
8. J. R. Teijaro, D. Turner, Q. Pham, E. J. Wherry, L. Lefrançois, D. L. Farber, Cutting edge: Tissue-retentive lung memory CD4 T cells mediate optimal protection to respiratory virus infection. *J. Immunol.* **187**, 5510–5514 (2011).
9. H. Shin, A. Iwasaki, A vaccine strategy that protects against genital herpes by establishing local memory T cells. *Nature* **491**, 463–467 (2012).
10. D. Masopust, D. Choo, V. Vezys, E. J. Wherry, J. Duraiswamy, R. Akondy, J. Wang, K. A. Casey, D. L. Barber, K. S. Kawamura, K. A. Fraser, R. J. Webby, V. Brinkmann, E. C. Butcher, K. A. Newell, R. Ahmed, Dynamic T cell migration program provides resident memory within intestinal epithelium. *J. Exp. Med.* **207**, 553–564 (2010).
11. R. Bartolomé-Casado, O. J. B. Landsverk, S. K. Chauhan, L. Richter, D. Phung, V. Greiff, L. F. Risnes, Y. Yao, R. S. Neumann, S. Yaqub, O. Øyen, R. Horneland, E. M. Aandahl, V. Paulsen, L. M. Sollid, S.-W. Qiao, E. S. Baekkevold, F. L. Jahnsen, Resident memory CD8 T cells persist for years in human small intestine. *J. Exp. Med.* **216**, 2412–2426 (2019).
12. S. L. Park, A. Buzzai, J. Rautela, J. L. Hor, K. Hochheiser, M. Effern, N. McBain, T. Wagner, J. Edwards, R. McConville, J. S. Wilmott, R. A. Scolyer, T. Tüting, U. Palendira, D. Gyorki, S. N. Mueller, N. D. Huntington, S. Bedoui, M. Hölzel, L. K. Mackay, J. Waithman, T. Gebhardt, Tissue-resident memory CD8$^+$ T cells promote melanoma–immune equilibrium in skin. *Nature* **565**, 366–371 (2019).
13. C. Li, B. Zhu, Y. M. Son, Z. Wang, L. Jiang, M. Xiang, Z. Ye, K. E. Beckermann, Y. Wu, J. W. Jenkins, P. J. Siska, B. G. Vincent, Y. S. Prakash, T. Peikert, B. T. Edelson, R. Taneja, M. H. Kaplan, J. C. Rathmell, H. Dong, T. Hitosugi, J. Sun, The transcription factor bhlhe40 programs mitochondrial regulation of resident CD8$^+$ T cell fitness and functionality. *Immunity* **51**, 491–507.e7 (2019).
14. P. Savas, B. Virassamy, C. Ye, A. Salim, C. P. Mintoff, F. Caramia, R. Salgado, D. J. Byrne, Z. L. Teo, S. Dushyanthen, A. Byrne, L. Wein, S. J. Luen, C. Poliness, S. S. Nightingale, A. S. Skandarajah, D. E. Gyorki, C. M. Thornton, P. A. Beavis, S. B. Fox; Kathleen Cuningham Foundation Consortium for Research into Familial Breast Cancer (kConFab), P. K. Darcy, T. P. Speed, L. K. Mackay, P. J. Neeson, S. Loi, Single-cell profiling of breast cancer T cells reveals a tissue-resident memory subset associated with improved prognosis. *Nat. Med.* **24**, 986–993 (2018).
15. C. O. Park, T. S. Kupper, The emerging role of resident memory T cells in protective immunity and inflammatory disease. *Nat. Med.* **21**, 688–697 (2015).

Downloaded from https://www.science.org at American University of Beirut on April 16, 2024

16. O. Boyman, H. P. Hefti, C. Conrad, B. J. Nickoloff, M. Suter, F. O. Nestle, Spontaneous development of psoriasis in a new animal model shows an essential role for resident T cells and tumor necrosis factor-alpha. *J. Exp. Med.* **199**, 731–736 (2004).
17. S. Zundler, E. Becker, M. Spocinska, M. Slawik, L. Parga-Vidal, R. Stark, M. Wiendl, R. Atreya, T. Rath, M. Leppkes, K. Hildner, R. López-Posadas, S. Lukassen, A. B. Ekici, C. Neufert, I. Atreya, K. P. J. M. van Gisbergen, M. F. Neurath, Hobit- and Blimp-1-driven $CD4^+$ tissue-resident memory T cells control chronic intestinal inflammation. *Nat. Immunol.* **20**, 288–300 (2019).
18. F. G. Lakkis, A. Arakelov, B. T. Konieczny, Y. Inoue, Immunologic 'ignorance' of vascularized organ transplants in the absence of secondary lymphoid tissue. *Nat. Med.* **6**, 686–688 (2000).
19. G. Chalasani, Z. Dai, B. T. Konieczny, F. K. Baddoura, F. G. Lakkis, Recall and propagation of allospecific memory T cells independent of secondary lymphoid organs. *Proc. Natl. Acad. Sci. U.S.A.* **99**, 6175–6180 (2002).
20. S. Ibrahim, D. V. Dawson, F. Sanfilippo, Predominant infiltration of rejecting human renal allografts with T cells expressing CD8 and CD45RO. *Transplantation* **59**, 724–728 (1995).
21. A. D. Hughes, D. Zhao, H. Dai, K. I. Abou-Daya, R. Tieu, R. Rammal, A. L. Williams, D. P. Landsittel, W. D. Shlomchik, A. E. Morelli, M. H. Oberbarnscheidt, F. G. Lakkis, Cross-dressed dendritic cells sustain effector T cell responses in islet and kidney allografts. *J. Clin. Invest.* **130**, 287–294 (2020).
22. E. B. Thorp, C. Stehlik, M. J. Ansari, T-cell exhaustion in allograft rejection and tolerance. *Curr. Opin. Organ Transplant.* **20**, 37–42 (2015).
23. E. J. Wherry, M. Kurachi, Molecular and cellular insights into T cell exhaustion. *Nat. Rev. Immunol.* **15**, 486–499 (2015).
24. K. Tanaka, M. J. Albin, X. Yuan, K. Yamaura, A. Habicht, T. Murayama, M. Grimm, A. M. Waaga, T. Ueno, R. F. Padera, H. Yagita, M. Azuma, T. Shin, B. R. Blazar, D. M. Rothstein, M. H. Sayegh, N. Najafian, PDL1 is required for peripheral transplantation tolerance and protection from chronic allograft rejection. *J. Immunol.* **179**, 5204–5210 (2007).
25. D. Zou, Y. Dai, X. Zhang, G. Wang, X. Xiao, P. Jia, X. C. Li, Z. Guo, W. Chen, T cell exhaustion is associated with antigen abundance and promotes transplant acceptance. *Am. J. Transplant.* **20**, 2540–2550 (2020).
26. B. H. Koehn, M. L. Ford, I. R. Ferrer, K. Borom, S. Gangappa, A. D. Kirk, C. P. Larsen, PD-1-dependent mechanisms maintain peripheral tolerance of donor-reactive $CD8^+$ T cells to transplanted tissue. *J. Immunol.* **181**, 5313–5322 (2008).
27. J. Zuber, B. Shonts, S. P. Lau, A. Obradovic, J. Fu, S. Yang, M. Lambert, S. Coley, J. Weiner, J. Thome, S. DeWolf, D. L. Farber, Y. Shen, S. Caillat-Zucman, G. Bhagat, A. Griesemer, M. Martinez, T. Kato, M. Sykes, Bidirectional intragraft alloreactivity drives the repopulation of human intestinal allografts and correlates with clinical outcome. *Sci. Immunol.* **1**, eaah3732 (2016).
28. M. E. Snyder, M. O. Finlayson, T. J. Connors, P. Dogra, T. Senda, E. Bush, D. Carpenter, C. Marboe, L. Benvenuto, L. Shah, H. Robbins, J. L. Hook, M. Sykes, F. D'Ovidio, M. Bacchetta, J. R. Sonett, D. J. Lederer, S. Arcasoy, P. A. Sims, D. L. Farber, Generation and persistence of human tissue-resident memory T cells in lung transplantation. *Sci. Immunol.* **4**, eaav5581 (2019).
29. K. de Leur, M. Dieterich, D. A. Hesselink, O. B. J. Corneth, F. J. M. F. Dor, G. N. de Graav, A. M. A. Peeters, A. Mulder, H. J. A. N. Kimenai, F. H. J. Claas, M. C. Clahsen-van Groningen, L. J. W. van der Laan, R. W. Hendriks, C. C. Baan, Characterization of donor and recipient $CD8^+$ tissue-resident memory T cells in transplant nephrectomies. *Sci. Rep.* **9**, 5984 (2019).
30. R. B. Mannon, J. B. Kopp, P. Ruiz, R. Griffiths, M. Bustos, J. L. Platt, P. E. Klotman, T. M. Coffman, Chronic rejection of mouse kidney allografts. *Kidney Int.* **55**, 1935–1944 (1999).
31. M. Miyajima, C. M. Chase, A. Alessandrini, E. A. Farkash, P. Della Pelle, G. Benichou, J. A. Graham, J. C. Madsen, P. S. Russell, R. B. Colvin, Early acceptance of renal allografts in mice is dependent on foxp3(+) cells. *Am. J. Pathol.* **178**, 1635–1645 (2011).
32. B. D. Ehst, E. Ingulli, M. K. Jenkins, Development of a novel transgenic mouse for the study of interactions between CD4 and CD8 T cells during graft rejection. *Am. J. Transplant.* **3**, 1355–1362 (2003).
33. J. J. Milner, C. Toma, B. Yu, K. Zhang, K. Omilusik, A. T. Phan, D. Wang, A. J. Getzler, T. Nguyen, S. Crotty, W. Wang, M. E. Pipkin, A. W. Goldrath, Runx3 programs $CD8^+$ T cell residency in non-lymphoid tissues and tumours. *Nature* **552**, 253–257 (2017).
34. C. N. Skon, J. Y. Lee, K. G. Anderson, D. Masopust, K. A. Hogquist, S. C. Jameson, Transcriptional downregulation of S1pr1 is required for the establishment of resident memory $CD8^+$ T cells. *Nat. Immunol.* **14**, 1285–1293 (2013).
35. E. J. Wherry, S. J. Ha, S. M. Kaech, W. N. Haining, S. Sarkar, V. Kalia, S. Subramaniam, J. N. Blattman, D. L. Barber, R. Ahmed, Molecular signature of CD8+ T cell exhaustion during chronic viral infection. *Immunity* **27**, 670–684 (2007).
36. L. Kok, F. E. Dijkgraaf, J. Urbanus, K. Bresser, D. W. Vredevoogd, R. F. Cardoso, L. Perié, J. B. Beltman, T. N. Schumacher, A committed tissue-resident memory T cell precursor within the circulating CD8+ effector T cell pool. *J. Exp. Med.* **217**, (2020).
37. B. V. Kumar, W. Ma, M. Miron, T. Granot, R. S. Guyer, D. J. Carpenter, T. Senda, X. Sun, S. H. Ho, H. Lerner, A. L. Friedman, Y. Shen, D. L. Farber, Human tissue-resident memory T cells are defined by core transcriptional and functional signatures in lymphoid and mucosal sites. *Cell Rep.* **20**, 2921–2934 (2017).
38. L. M. Wakim, J. Waithman, N. van Rooijen, W. R. Heath, F. R. Carbone, Dendritic cell-induced memory T cell activation in nonlymphoid tissues. *Science* **319**, 198–202 (2008).
39. P. A. Szabo, M. Miron, D. L. Farber, Location, location, location: Tissue resident memory T cells in mice and humans. *Sci. Immunol.* **4**, eaas9673 (2019).
40. E. J. Suchin, P. B. Langmuir, E. Palmer, M. H. Sayegh, A. D. Wells, L. A. Turka, Quantifying the frequency of alloreactive T cells in vivo: New answers to an old question. *J. Immunol.* **166**, 973–981 (2001).
41. C. Macedo, E. A. Orkis, I. Popescu, B. D. Elinoff, A. Zeevi, R. Shapiro, F. G. Lakkis, D. Metes, Contribution of naïve and memory T-cell populations to the human alloimmune response. *Am. J. Transplant.* **9**, 2057–2066 (2009).
42. L. M. McLane, M. S. Abdel-Hakeem, E. J. Wherry, CD8 T cell exhaustion during chronic viral infection and cancer. *Annu. Rev. Immunol.* **37**, 457–495 (2019).
43. Z. Wang, S. Wang, N. P. Goplen, C. Li, I. S. Cheon, Q. Dai, S. Huang, J. Shan, C. Ma, Z. Ye, M. Xiang, A. H. Limper, E. C. Porquera, J. E. Kohlmeier, M. H. Kaplan, N. Zhang, A. J. Johnson, R. Vassallo, J. Sun, PD-1hiCD8+ resident memory T cells balance immunity and fibrotic sequelae. *Sci. Immunol.* **4**, eaaw1217 (2019).
44. B. C. Miller, D. R. Sen, R. al Abosy, K. Bi, Y. V. Virkud, M. W. LaFleur, K. B. Yates, A. Lako, K. Felt, G. S. Naik, M. Manos, E. Gjini, J. R. Kuchroo, J. J. Ishizuka, J. L. Collier, G. K. Griffin, S. Maleri, D. E. Comstock, S. A. Weiss, F. D. Brown, A. Panda, M. D. Zimmer, R. T. Manguso, F. S. Hodi, S. J. Rodig, A. H. Sharpe, W. N. Haining, Subsets of exhausted $CD8^+$ T cells differentially mediate tumor control and respond to checkpoint blockade. *Nat. Immunol.* **20**, 326–336 (2019).
45. S. Kurtulus, A. Madi, G. Escobar, M. Klapholz, J. Nyman, E. Christian, M. Pawlak, D. Dionne, J. Xia, O. Rozenblatt-Rosen, V. K. Kuchroo, A. Regev, A. C. Anderson, Checkpoint blockade immunotherapy induces dynamic changes in PD-1^-CD8^+ tumor-infiltrating T cells. *Immunity* **50**, 181–194.e6 (2019).
46. I. Siddiqui, K. Schaeuble, V. Chennupati, S. A. F. Marraco, S. Calderon-Copete, D. P. Ferreira, S. J. Carmona, L. Scarpellino, D. Gfeller, S. Pradervand, S. A. Luther, D. E. Speiser, W. Held, Intratumoral $Tcf1^+PD\text{-}1^+CD8^+$ T cells with stem-like properties promote tumor control in response to vaccination and checkpoint blockade immunotherapy. *Immunity* **50**, 195–211.e10 (2019).
47. D. L. Barber, E. J. Wherry, D. Masopust, B. Zhu, J. P. Allison, A. H. Sharpe, G. J. Freeman, R. Ahmed, Restoring function in exhausted CD8 T cells during chronic viral infection. *Nature* **439**, 682–687 (2006).
48. G. A. Hadley, S. T. Bartlett, C. S. Via, E. A. Rostapshova, S. Moainie, The epithelial cell-specific integrin, CD103 (alpha E integrin), defines a novel subset of alloreactive CD8+ CTL. *J. Immunol.* **159**, 3748–3756 (1997).
49. Y. Feng, D. Wang, R. Yuan, C. M. Parker, D. L. Farber, G. A. Hadley, CD103 expression is required for destruction of pancreatic islet allografts by CD8+ T cells. *J. Exp. Med.* **196**, 877–886 (2002).
50. R. Yuan, R. el-Asady, K. Liu, D. Wang, C. B. Drachenberg, G. A. Hadley, Critical role for $CD103^+CD8^+$ effectors in promoting tubular injury following allogeneic renal transplantation. *J. Immunol.* **175**, 2868–2879 (2005).
51. L. Zhang, S. D. Moffatt-Bruce, A. A. Gaughan, J. J. Wang, A. Rajab, G. A. Hadley, An anti-CD103 immunotoxin promotes long-term survival of pancreatic islet allografts. *Am. J. Transplant.* **9**, 2012–2023 (2009).
52. L. K. Beura, S. E. Hamilton, K. Bi, J. M. Schenkel, O. A. Odumade, K. A. Casey, E. A. Thompson, K. A. Fraser, P. C. Rosato, A. Filali-Mouhim, R. P. Sekaly, M. K. Jenkins, V. Vezys, W. N. Haining, S. C. Jameson, D. Masopust, Normalizing the environment recapitulates adult human immune traits in laboratory mice. *Nature* **532**, 512–516 (2016).
53. Q. Zhuang, Q. Liu, S. J. Divito, Q. Zeng, K. M. Yatim, A. D. Hughes, D. M. Rojas-Canales, A. Nakao, W. J. Shufesky, A. L. Williams, R. Humar, R. A. Hoffman, W. D. Shlomchik, M. H. Oberbarnscheidt, F. G. Lakkis, A. E. Morelli, Graft-infiltrating host dendritic cells play a key role in organ transplant rejection. *Nat. Commun.* **7**, 12623 (2016).
54. D. V. Sawant, H. Yano, M. Chikina, Q. Zhang, M. Liao, C. Liu, D. J. Callahan, Z. Sun, T. Sun, T. Tabib, A. Pennathur, D. B. Corry, J. D. Luketich, R. Lafyatis, W. Chen, A. C. Poholek, T. C. Bruno, C. J. Workman, D. A. A. Vignali, Adaptive plasticity of IL-10^+ and IL-35^+ Treg cells cooperatively promotes tumor T cell exhaustion. *Nat. Immunol.* **20**, 724–735 (2019).
55. C. Liu, A. Somasundaram, S. Manne, A. M. Gocher, A. L. Szymczak-Workman, K. M. Vignali, E. N. Scott, D. P. Normolle, E. John Wherry, E. J. Lipson, R. L. Ferris, T. C. Bruno, C. J. Workman, D. A. A. Vignali, Neuropilin-1 is a T cell memory checkpoint limiting long-term antitumor immunity. *Nat. Immunol.* **21**, 1010–1021 (2020).
56. Y. J. Shim, R. Khedraki, J. Dhar, R. Fan, N. Dvorina, A. Valujskikh, R. L. Fairchild, W. M. Baldwin III, Early T cell infiltration is modulated by programed cell death-1 protein and its ligand (PD-1/PD-L1) interactions in murine kidney transplants. *Kidney Int.* **98**, 897–905 (2020).

Downloaded from https://www.science.org at American University of Beirut on April 16, 2024

57. J. Mohammed, L. K. Beura, A. Bobr, B. Astry, B. Chicoine, S. W. Kashem, N. E. Welty, B. Z. Igyártó, S. Wijeyesinghe, E. A. Thompson, C. Matte, L. Bartholin, A. Kaplan, D. Sheppard, A. G. Bridges, W. D. Shlomchik, D. Masopust, D. H. Kaplan, Stromal cells control the epithelial residence of DCs and memory T cells by regulated activation of TGF-β. *Nat. Immunol.* **17**, 414–421 (2016).
58. C. Ma, S. Mishra, E. L. Demel, Y. Liu, N. Zhang, TGF-β controls the formation of kidney-resident T cells via promoting effector T cell extravasation. *J. Immunol.* **198**, 749–756 (2017).
59. P. Kamran, K.-I. Sereti, P. Zhao, S. R. Ali, I. L. Weissman, R. Ardehali, Parabiosis in mice: A detailed protocol. *J. Vis. Exp.* **2013**, 50556 (2013).
60. L. C. Bonifaz, D. P. Bonnyay, A. Charalambous, D. I. Darguste, S. I. Fujii, H. Soares, M. K. Brimnes, B. Moltedo, T. M. Moran, R. M. Steinman, In vivo targeting of antigens to maturing dendritic cells via the DEC-205 receptor improves T cell vaccination. *J. Exp. Med.* **199**, 815–824 (2004).
61. J. M. Walch, Q. Zeng, Q. Li, M. H. Oberbarnscheidt, R. A. Hoffman, A. L. Williams, D. M. Rothstein, W. D. Shlomchik, J. V. Kim, G. Camirand, F. G. Lakkis, Cognate antigen directs $CD8^+$ T cell migration to vascularized transplants. *J. Clin. Invest.* **123**, 2663–2671 (2013).
62. K. G. Anderson, K. Mayer-Barber, H. Sung, L. Beura, B. R. James, J. J. Taylor, L. Qunaj, T. S. Griffith, V. Vezys, D. L. Barber, D. Masopust, Intravascular staining for discrimination of vascular and tissue leukocytes. *Nat. Protoc.* **9**, 209–222 (2014).
63. M. H. Oberbarnscheidt, Q. Zeng, Q. Li, H. Dai, A. L. Williams, W. D. Shlomchik, D. M. Rothstein, F. G. Lakkis, Non-self recognition by monocytes initiates allograft rejection. *J. Clin. Invest.* **124**, 3579–3589 (2014).
64. C. Roufosse, N. Simmonds, M. Clahsen-van Groningen, M. Haas, K. J. Henriksen, C. Horsfield, A. Loupy, M. Mengel, A. Perkowska-Ptasińska, M. Rabant, L. C. Racusen, K. Solez, J. U. Becker, A 2018 reference guide to the Banff classification of renal allograft pathology. *Transplantation* **102**, 1795–1814 (2018).
65. G. Camirand, Q. Li, A. J. Demetris, S. C. Watkins, W. D. Shlomchik, D. M. Rothstein, F. G. Lakkis, Multiphoton intravital microscopy of the transplanted mouse kidney. *Am. J. Transplant.* **11**, 2067–2074 (2011).
66. S. Babicki, D. Arndt, A. Marcu, Y. Liang, J. R. Grant, A. Maciejewski, D. S. Wishart, Heatmapper: Web-enabled heat mapping for all. *Nucleic Acids Res.* **44**, W147–W153 (2016).
67. M. Stoeckius, S. Zheng, B. Houck-Loomis, S. Hao, B. Z. Yeung, W. M. Mauck III, P. Smibert, R. Satija, Cell hashing with barcoded antibodies enables multiplexing and doublet detection for single cell genomics. *Genome Biol.* **19**, 224 (2018).

Acknowledgments: We acknowledge M. Snyder at the University of Pittsburgh for helpful discussions and the Single Cell (T. Tabib and R. Lafyatis) and the Unified Flow Cytometry (L. Borghesi) cores at the University of Pittsburgh for the services. Partek Flow and IPA software are licensed through the Molecular Biology Information Service (A. Chattopadhyay) of the Health Sciences Library System, University of Pittsburgh. This research was supported in part by University of Pittsburgh Center for Research Computing (CRC) through the resources provided. **Funding:** This work was supported by NIH grants AI049466 to F.G.L., AI145881 to M.H.O., and HL143349 to W.D.S. K.I.A.-D. was funded by the American Society of Nephrology Ben J. Lipps Research Fellowship. R.T. was funded by T32 grant AI074490, F30 grant DK124925, and T32 grant GM008208 from the NIH. F.S. is the recipient of the Thomas E. Starzl Postdoctoral Fellowship in Transplantation Biology. The Unified Flow Cytometry Core is funded by NIH grants 1S10OD011925-01 and 1S10OD019942-01. **Author contributions:** K.I.A.-D., R.T., D.Z., and A.L.W. performed experiments. R.R. interpreted tissue pathology. A.L.W. maintained and genotyped mouse colonies. K.I.A.-D. analyzed scRNA-seq data. F.S. and W.D.S. provided experimental and intellectual input. M.H.O. and F.G.L. supervised the work and wrote the manuscript with K.I.A.-D. All the authors critically revised the manuscript for content. **Competing interests:** The authors declare that they have no competing interests. **Data and materials availability:** Raw scRNA-seq data have been deposited into the Gene Expression Omnibus (GEO) database (accession no. GSE166166). All other data needed to evaluate the conclusions of the paper are available in the manuscript or the Supplementary Materials.

Submitted 15 May 2020
Accepted 8 February 2021
Published 19 March 2021
10.1126/sciimmunol.abc8122

Citation: K. I. Abou-Daya, R. Tieu, D. Zhao, R. Rammal, F. Sacirbegovic, A. L. Williams, W. D. Shlomchik, M. H. Oberbarnscheidt, F. G. Lakkis, Resident memory T cells form during persistent antigen exposure leading to allograft rejection. *Sci. Immunol.* **6**, eabc8122 (2021).

Downloaded from https://www.science.org at American University of Beirut on April 16, 2024